



Article

Novel Furocoumarin Derivatives Stimulate Melanogenesis in B16 Melanoma Cells by Up-Regulation of MITF and TYR Family via Akt/GSK3 β / β -Catenin Signaling Pathways

Chao Niu ¹, Li Yin ^{1,2} and Haji Akber Aisa ^{1,*}

¹ Key Laboratory of Plant Resources and Chemistry of Arid Zone, State Key Laboratory Basis of Xinjiang Indigenous Medicinal Plants Resource Utilization, Xinjiang Technical Institute of Physics and Chemistry, Chinese Academy of Sciences, Urumqi 830011, China; niuchao@ms.xjb.ac.cn (C.N.); jinshiyi2003@163.com (L.Y.)

² University of Chinese Academy of Sciences, Beijing 101408, China

* Correspondence: haji@ms.xjb.ac.cn; Tel.: +86-0991-383-5679

Received: 15 January 2018; Accepted: 16 February 2018; Published: 6 March 2018

Abstract: The extracts of *Ficus carica* L. and *Psoralea corylifolia* L. are traditional Uygur medicines for the treatment of vitiligo, and its active ingredients furocoumarins, were are found to be the most effective agents against this skin disorder nowadays. Therefore, a series of novel ester derivatives (**8a–8p**) of furocoumarin were designed and synthesized based on our previous research to improve this activity in the present study. The synthesized derivatives were biologically evaluated for melanin synthesis in murine B16 cells and the SAR (structure-activity relationship) was summarized. Eight derivatives were more potent than positive control (8-MOP, 8-methoxypsoralan), especially compounds **8n** (200%) and **8o** (197%), which were nearly 1.5-fold potency when compared with 8-MOP (136%). Furthermore, the signaling pathway by which **8n** activates the melanin biosynthesis was defined. Our results showed that it not only elevated the melanin content, but also stimulated the activity of tyrosinase in a concentration-dependent manner. Increasing of phosphorylation of Akt (also named PKB, protein kinase B) and non-activated GSK3 β (glycogen synthase kinase 3 beta), which inhibited the degradation of β -catenin were observed through Western blot analysis. The accumulation of β -catenin probably led to the activation of transcription of MITF (microphthalmia-associated transcription factor) and TYR (tyrosinase) family, as well as the subsequent induction of melanin synthesis.

Keywords: vitiligo; furocoumarin; melanogenesis; SAR; Akt/GSK3 β / β -catenin signaling pathways

1. Introduction

Vitiligo also named leukoderma, is an autoimmune disease that results in prominent white patches of the skin [1]. It can involve any part of the body where melanocytes resided and cause both functional and physiological abnormalities in the affected skin. Many possible causes of vitiligo have been proposed including immunologic, genetic, stress, neural mechanism, and biochemical factors [2]. However, it is believed that the disease is mainly caused by destruction of the melanocyte and obstruction of the melanin synthesis [3,4].

Melanin, derived from dopaquinone and synthesized in the melanosomes of melanocytes, serves a number of valuable physiological functions [5]. The melanin biosynthesis is regulated by enzymatic cascade, such as tyrosinase, tyrosinase-related protein 1 (TRP-1) and tyrosinase-related protein 2 (TRP-2) [6]. Among them, tyrosinase is regarded as the rate-limiting enzyme of process, which modulates this process by catalyzing the hydroxylation of tyrosine into 3,4-dihydroxyphenylalanine (DOPA) and the further oxidation of DOPA into dopaquinone [7,8].

Several signaling pathways are presented to clarify the specific mechanism controlling melanin biosynthesis via tyrosinase family, as described in Figure 1 [9,10]. MITF, a master regulator of melanogenesis that is involved in these pathways, upregulates the melanogenesis enzymes TYR, TRP-1 and TRP-2 via binding to the M-box motif in their promoter regions [11]. In addition, MITF modulates melanocyte function including melanocyte differentiation, pigmentation, proliferation, and cell survival [12].

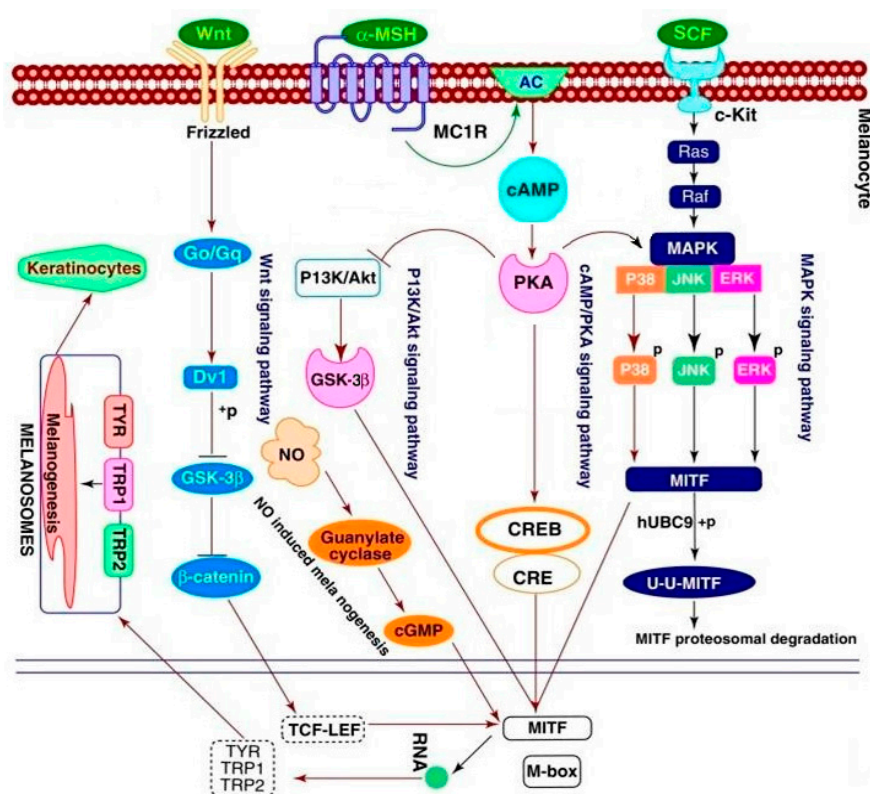


Figure 1. Regulation of melanogenesis through different signaling pathways [10]. α -MSH (α -melanocyte-stimulating hormone), SCF (stem cell factor), AC (adenylate cyclase), MC1R (melanocortin 1 receptor), cAMP (cyclic Adenosine monophosphate), PKA (protein kinase A), MAPK (mitogen-activated protein kinase), GSK (glycogen synthase kinase), JNK (c-Jun N-terminal kinase), ERK (extracellular regulated protein kinases), TYR (tyrosinase), TRP1 (Tyrosinase-related protein 1), TRP2 (Tyrosinase-related protein 2) CREB (cAMP-response element binding protein), CRE (cAMP response element), MITF (microphthalmia-associated transcription factor), TCF-LEF (T cell factor/lymphoid-enhancing factor-1).

The extract of *Ficus carica* L. and *Psoralea corylifolia* L. (Figure 2) [13,14] alone or in combination are popular Uyghur medicines that are used for vitiligo in Xinjiang and other Central Asian countries hundreds of years ago [15,16]. During the last century, several furocoumarins (psoralens), such as 8-methoxypsoralen (8-MOP), 5-methoxypsoralen (5-MOP), and 4,5,8-trimethylpsoralen (TMP) were isolated from the plants or totally synthesized [17,18]. These compounds were proved to show strong photosensitivity [19] later, which may be used for the treatment of vitiligo with subsequent exposure to long-waved ultraviolet radiation [20,21]. Although PUVA (psoralens + UVA) (ultraviolet radiation A) [22] was accompanied with some undesired side effects [23–25], the therapy is still the most successful (or less disappointing) one for skin repigmentation today. Unfortunately, the precise mechanism of PUVA in the treatment of vitiligo is obscure, let alone the target of these drugs.

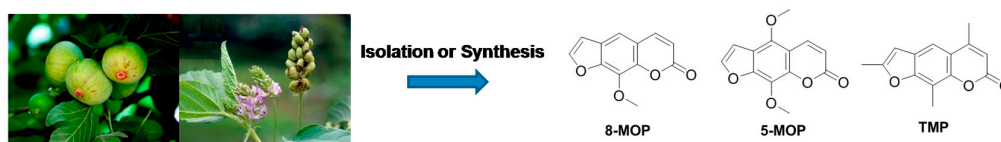


Figure 2. The structures of furocoumarins (psoralens) isolated from the plant *Ficus carica* L. and *Psoralea corylifolia* L. or synthesized [13]. 5-MOP (5-methoxypsoralen), TMP (trimethylpsoralen).

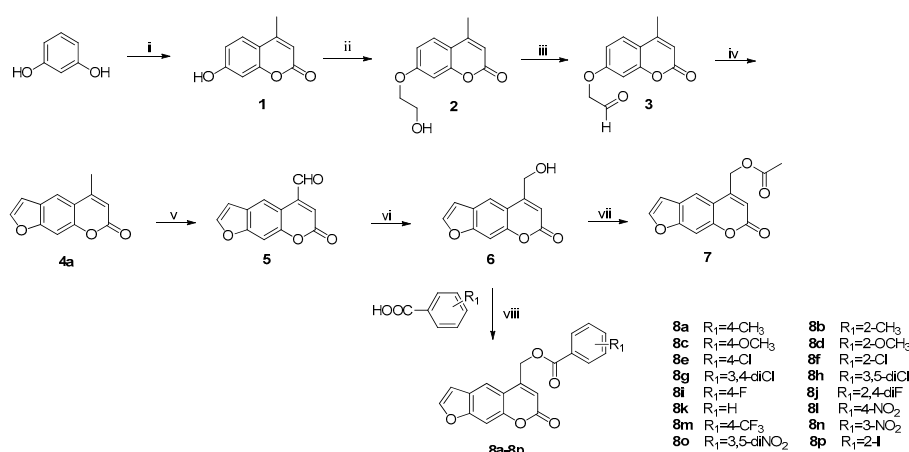
However, few furocoumarin derivatives and analogues with potential anti-vitiligo activity were reported in spite of their high efficiency against the disease. Our group had been dedicated on the drug development of the vitiligo for many years [26–31]. In our previous research, a great augmentation to the melanin synthesis was observed when aromatic groups were introduced to C-5 position of the furocoumarin derivative, which suggested that more structural modification should be pursued on this position to search for novel bioactive molecules on pigmentation that may be developed as better medication for the vitiligo.

Therefore, sixteen ester derivatives (**8a–8p**) of furocoumarin were prepared, then submitted to the activity assay of melanogenesis in B16 cells and the SAR was summarized as well. Furthermore, the tyrosinase activity and expression of proteins related to melanin biosynthesis were determined by Western blot analysis in cells treated with the most promising derivative (**8n**) for understanding the mechanism underlying the observed effect.

2. Results and Discussion

2.1. Synthesis

The synthetic route of the target compounds was described in Scheme 1. The intermediate **1** (4-methylumbelliferone) prepared from resorcinol via Pechmann reaction [32,33], was converted to compound **2** by Williamson reaction refluxing with chloroethanol in the presence of anhydrous K_2CO_3 . Compound **2** was further oxidized to aldehyde **3** at $-78^\circ C$ by an optimized Swern oxidation in excellent yields. Intermolecular cycloaddition of the intermediate **3** yielded compound **4a** in the presence of 1M NaOH. It is notable that a mixed solvent ($V_{\text{water}}:V_{1,4\text{-dioxane}} = 1:1$) was applied to get a homogeneous solution of aldehyde **3** for the easy cycloaddition.



Scheme 1. Synthetic route for the furocoumarin derivatives (i) ethyl acetoacetate, H_2SO_4 , $60^\circ C$; (ii) chloroethanol, K_2CO_3 , acetone, reflux; (iii) $-78^\circ C$, oxalyl chloride, DMSO (dimethyl sulfoxide), triethylamine, DCM (dichloromethane); (iv) 1M NaOH aqueous solution, 1,4-dioxane; (v) SeO_2 , xylene, reflux; and, (vi) $NaBH_4$, ethanol, rt; (vii) pyridine, Ac_2O , rt. (viii) DCC (dicyclohexylcarbodiimide), DMAP (4-dimethylaminopyridine), DCM, $0^\circ C$ -rt (room temperature).

Selenium dioxide was applied in selective oxidation of compound **4a** to produce aldehyde **5**. Compound **5** was reduced with NaBH₄ to achieve alcohol **6** [34,35], which was further esterified to give **7** and **8a–8p** under different conditions, respectively [32,36].

The oxidation of intermediate **2** to **3** was the crucial step in the preparation of compounds **4a**, which bearing no substituent group on the furan ring. With the application of DMSO-(COCl)₂ oxidation system, compound **2** was smoothly transformed to aldehyde **3** in almost quantitative yield as we did in our previous work. In the cyclization of intermediate **3**, two sets of compounds (psoralen: **4a** and angelicin: **4b**) were produced in one step, which was isomer to each other (Figure 3). The yield of **4a** in the mixture was much higher than angelicin (**4b**) under basic condition.

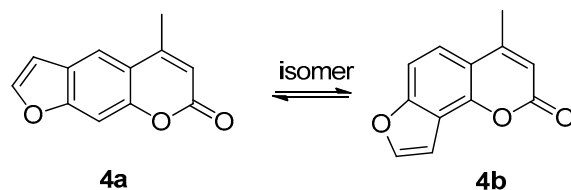


Figure 3. Structure of psoralen **4a** and angelicin **4b**.

2.2. Melanin Synthesis Evaluation of **8a–8p**

All of the synthesized compounds were screened for their activity on melanin synthesis in murine B16 cells, with a known method (Figure 4) [37]. In order to avoid the possibility that inhibition of melanin synthesis was due to cytotoxicity, we performed CCK-8 assay as well to determine whether these active ones were cytotoxic to B16 cells. The result showed that the cells treated with compounds for 48 h caused little cytotoxicity when compared with the control at the dosage of 50 μM (Figure 5).

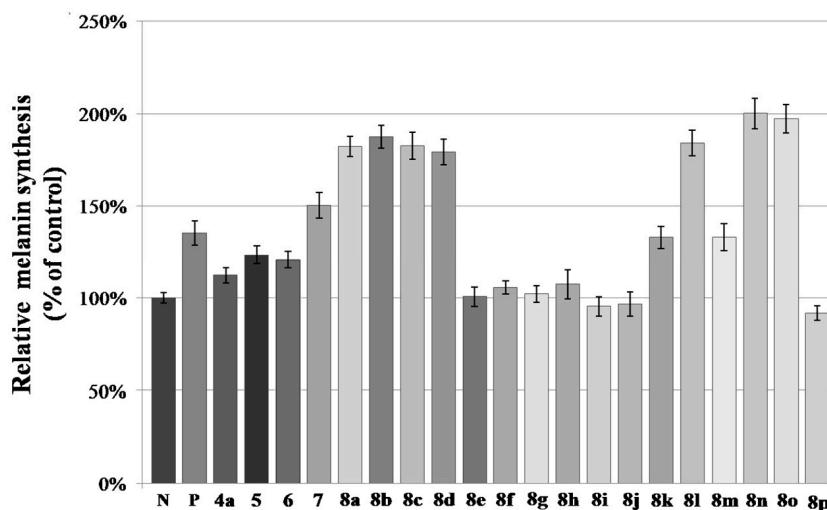


Figure 4. Stimulation of melanin content of B16 cells by furocoumarin derivatives. N means negative control; P means positive control (8-MOP); The B16 cells were treated with 50 μM of different furocoumarin derivatives for 48 h. After that, melanin content was measured directly. Values are expressed as the mean ± SD of three separate experiments.

According to the result (Figure 4), half of the tested compounds (**7**, **8a–8d**, **8l**, **8n–8o**) exhibited a stronger activity than the positive control (8-MOP) with a value from 182% to 200%. For compounds **6** and **7**, further esterification of hydroxymethyl with acetic anhydride caused an increase in activity.

The activity of ester derivatives, which substituted by halogens, decreased dramatically (**8e–8j**, **8p**) as compared with **8k**, especially for the ones bearing F and I, regardless of the number and position of halogens on benzene. Compounds with -CH₃ (**8a–8b**) and -OCH₃ (**8c–8d**) on *ortho*- and *para*-

position of benzene showed a much higher activity than the halogenated ones, which was consistent with our previous findings [28]. The interesting thing was that the strong electron-withdrawing group (EWG), such as $-\text{NO}_2$, may be favorable to promote the melanin content, especially for **8n** (200%) and **8o** (197%), which demonstrated the best activity of these derivatives. It seemed that this effect had no relationship with the position and number of the $-\text{NO}_2$ on benzene.

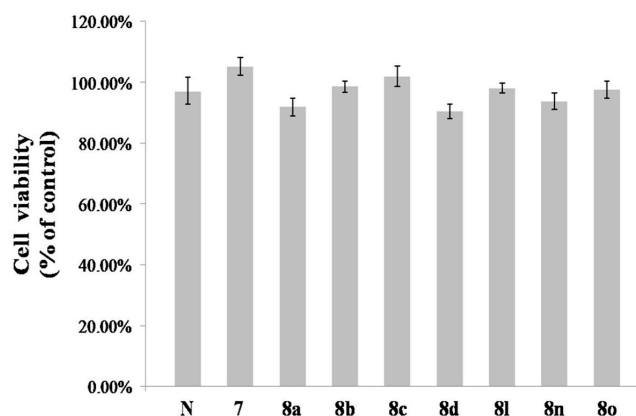


Figure 5. Effect of furocoumarin derivatives on B16 cells viability. N means negative control; The B16 cells were incubated with $50 \mu\text{M}$ of different furocoumarin derivatives for 48 h and the cell viability was assayed by adding CCK-8 (Cell Counting Kit) solution. Values are expressed as the mean \pm SD of three separate experiments.

Overall, both EDG (electron-donating group) ($-\text{CH}_3$, $-\text{OCH}_3$) and EWG ($-\text{NO}_2$) on benzene greatly improved the melanin biosynthesis, which indicated that the electrostatic interaction between derivatives and receptor protein may have little correlation with activity.

2.3. Effect of **8n** on B16 Melanoma Cells Viability

The murine melanoma B16 cells were treated with **8n** at concentrations of 0 – $50 \mu\text{M}$ for 24 h and examined the cytotoxicity by CCK-8 assay. As shown in Figure 6A(a–d), compound **8n** did not induce any change in cell morphology when compared with untreated cells and showed no increase in cytotoxicity (Figure 6B). Accordingly, 0 – $50 \mu\text{M}$ **8n** was applied in the subsequent experiments.

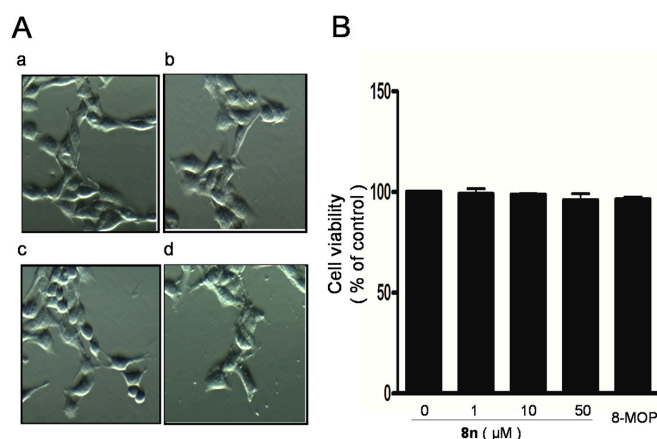


Figure 6. (A(a–d)) Effects of **8n** on cell morphology. B16 cells were treated with 0.1% DMSO (dimethyl sulfoxide) as vehicle (a) or with **8n** at 1 (b), 10 (c) and $50 \mu\text{M}$ (d) for 48 h. Cell morphology was observed under a microscope. Magnification, $\times 200$. (B) Effects of **8n** on B16 melanoma cell viability. B16 cells were treated with $50 \mu\text{M}$ 8-MOP as post control and with **8n** at concentrations of 0 – $50 \mu\text{M}$ for 48 h. Cell viability was measured by Cell Counting Kit-8 assays. The data are shown as the mean \pm SD; $n = 3$.

2.4. Effect of **8n** on Melanogenesis and Tyrosinase in B16 Melanoma Cells

The melanin production was measured in B16 melanoma cells after 48 h of treatment with **8n** at 0–50 μM . As shown in Figure 7A, treatment with **8n** improved the melanin synthesis in a dose-dependent manner, and the melanin content increased 63% compared with 8-MOP at 50 μM . (0 μM , $100 \pm 15.4\%$; 1 μM , $89.7 \pm 4.0\%$; 10 μM , $125.9 \pm 3.7\%$; 50 μM , $217.6 \pm 7.5\%$; 8-MOP, 50 μM , $133.5 \pm 12.1\%$). After that, the tyrosinase activity in B16 cells was studied as well and it showed a similar increasing trend in response to **8n** treatment in Figure 7B. Specifically, when compared with 8-MOP treated cells, treatment with compound at a concentration of 50 μM resulted in an approximately 98% activation of intracellular tyrosinase in the B16 melanoma cells. (0 μM , $100 \pm 9.2\%$; 1 μM , $150.7 \pm 8.7\%$; 10 μM , $192.4 \pm 6.4\%$; 50 μM , $293.9 \pm 4.3\%$; 8-MOP, 50 μM , $148.4 \pm 12.9\%$).

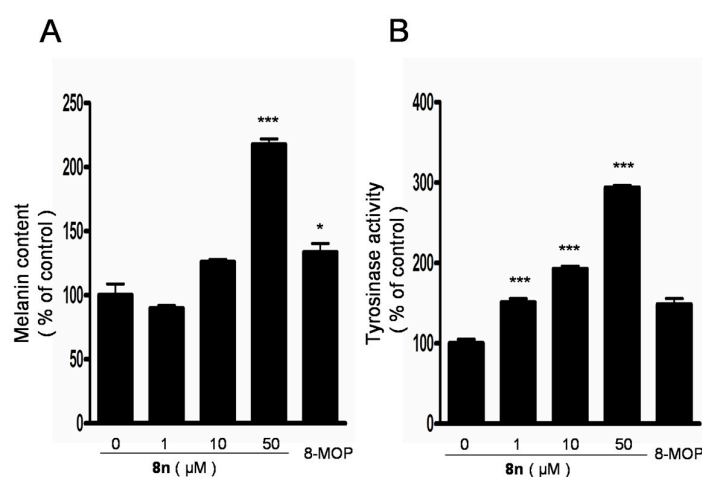


Figure 7. (A,B) Effects of **8n** on melanogenesis and tyrosinase in B16 melanoma cells. Cells were treated with 0.1% DMSO as vehicle or with **8n** at 1, 10, 50 μM , and 50 μM 8-MOP as positive control for 48 h or 24 h to evaluate melanin content and tyrosinase activity, respectively. Each percentage value for treated cells is reported relative to that of 0.1% DMSO cells. The data are shown as the mean \pm SD; $n = 3$, * $p < 0.05$, *** $p < 0.001$ as compared with 0.1% DMSO cells.

2.5. Effects of **8n** on TYR Family and MITF Expression Levels in B16 Melanoma Cells

In order to clarify the mechanism that is responsible for the elevation in pigmentation, the expression levels of TYR family and MITF were examined by Western blot. B16 melanoma cells were treated with various concentrations of **8n** (0–50 μM) for 48 h. As shown in Figure 8, the tyrosinase, TRP-1, and TRP-2 levels markedly increased following treatment with **8n**. As the TYR family was the downstream genes of MITF, the level of MITF was measured, and MITF expression exhibited comparative changes. These results suggested that **8n** induced melanin synthesis through the up-regulation of the TYR family and MITF at protein levels.

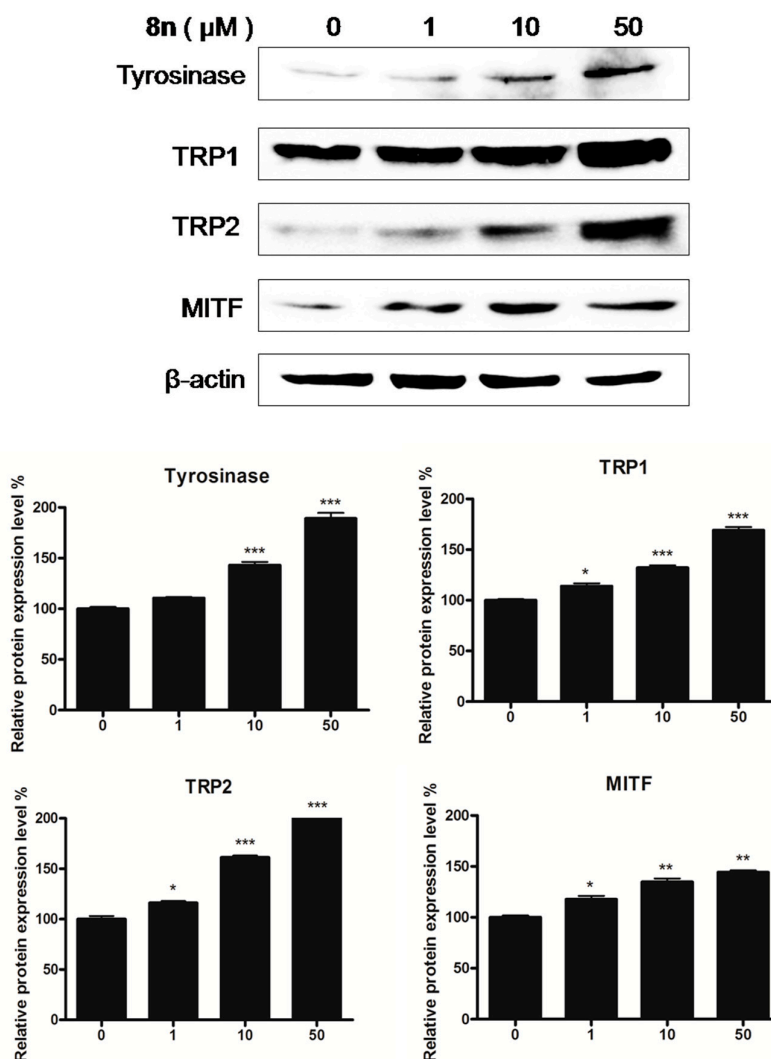


Figure 8. Representative western blots illustrating expression of TRPs and MITF. B16 cells were treated with **8n** at 0, 1, 10 and 50 μM for 48 h. Tyrosinase, TRP1, TRP2, and MITF protein expression were detected by Western blotting. Results were normalized against β -actin expression; Densitometric scanning of band intensities obtained from three individual experiments was used to quantify change of protein expression (control value taken as one-fold in each case). The Data are shown as mean \pm SD of three independent experiments. * $p < 0.05$, ** $p < 0.01$, *** $p < 0.001$ vs. controls.

2.6. Effect of **8n** on Akt and Wnt/ β -Catenin Signaling Pathways Involved in Melanogenesis

The Wnt signaling pathway was demonstrated as one of the signaling processes in melanin synthesis [38,39]. In order to determine the molecular mechanism of the superior pigmented effect of **8n**, Western blot analysis for the changes of β -catenin was introduced. As shown in Figure 9A, the phosphorylation of β -catenin at Ser33, decreased with a concomitant increase of total β -catenin induced by **8n**. Moreover, β -catenin content in the nucleus (the active β -catenin) enhanced obviously after 12 h of **8n** treatment as compared with untreated cells, while the content in the cytoplasm did not change (Figure 9B).

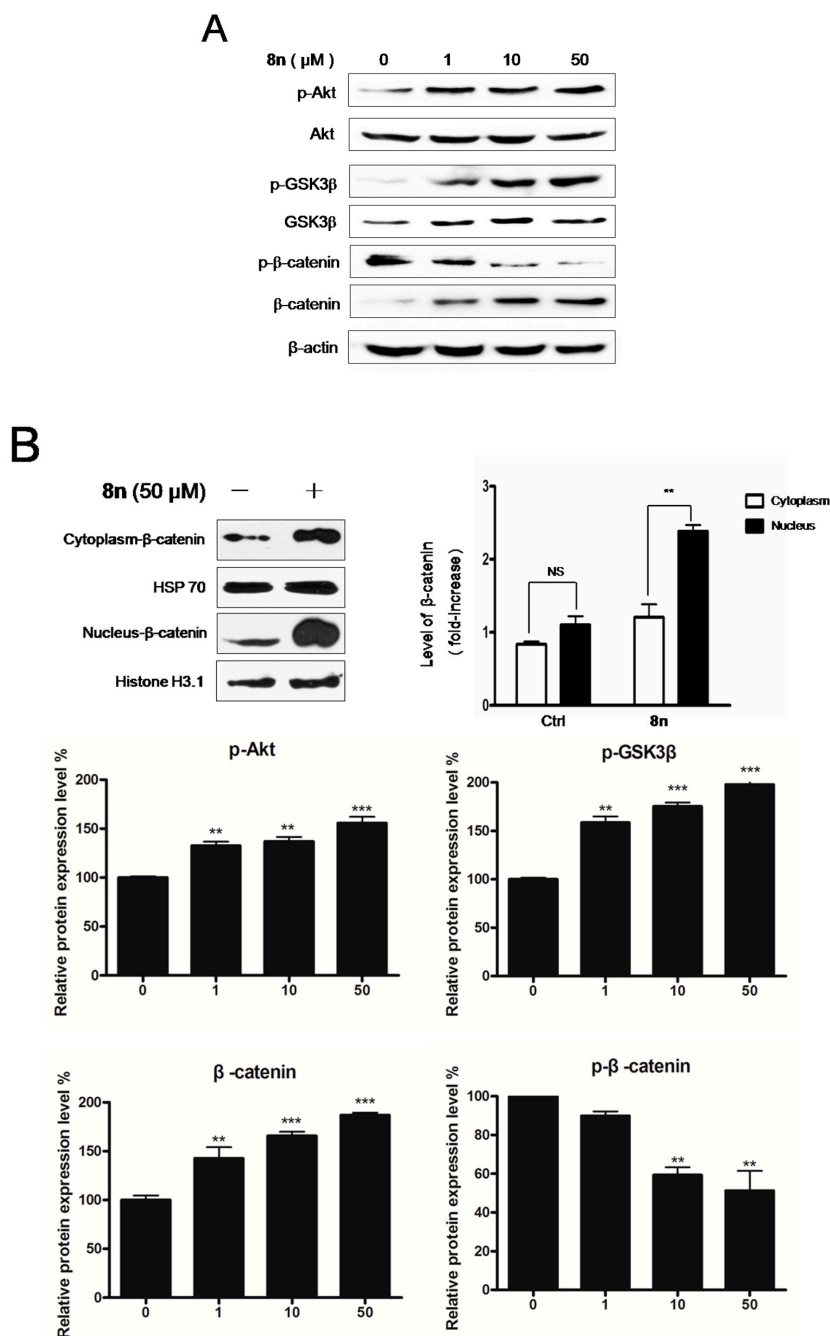


Figure 9. Effect of **8n** on Akt and Wnt/ β -catenin signaling pathways involved in melanogenesis. (A) B16 cells were treated with **8n** at the 0, 1, 10, and 50 μ M for 48 h, the expression of Akt, GSK3 β and β -catenin were measured by Western blot. (B) B16 cells were treated with **8n** of 50 μ M for 12 h, the expression levels of proteins including β -catenin in cytoplasm and nucleus were detected by using Western blot; Densitometric scanning of band intensities obtained from three individual experiments was used to quantify change of protein expression (control value taken as one-fold in each case). The Data are shown as mean \pm SD of three independent experiments. * $p < 0.05$, ** $p < 0.01$, *** $p < 0.001$ vs. controls.

GSK3 β , which is a negative regulator of Wnt signaling, could phosphorylate the residues of β -catenin, which contributes to the degradation of β -catenin through proteasome [40]. As expected, the level of phosphorylation of GSK3 β rose up in B16 cells treated with **8n** (Figure 9A). BIO (6-bromindirubin-3-oxime) was able to inhibit the phosphorylation of GSK3 β and regarded as

a selective GSK3 β inhibitor [41]. The graph revealed that the BIO increased the accumulation of β -catenin content induced by 8n (Figure 10A). Being consistent with this, it also improved the TYR activity and melanin content in B16 cells in the presence of 8n evidently (Figure 10B,C).

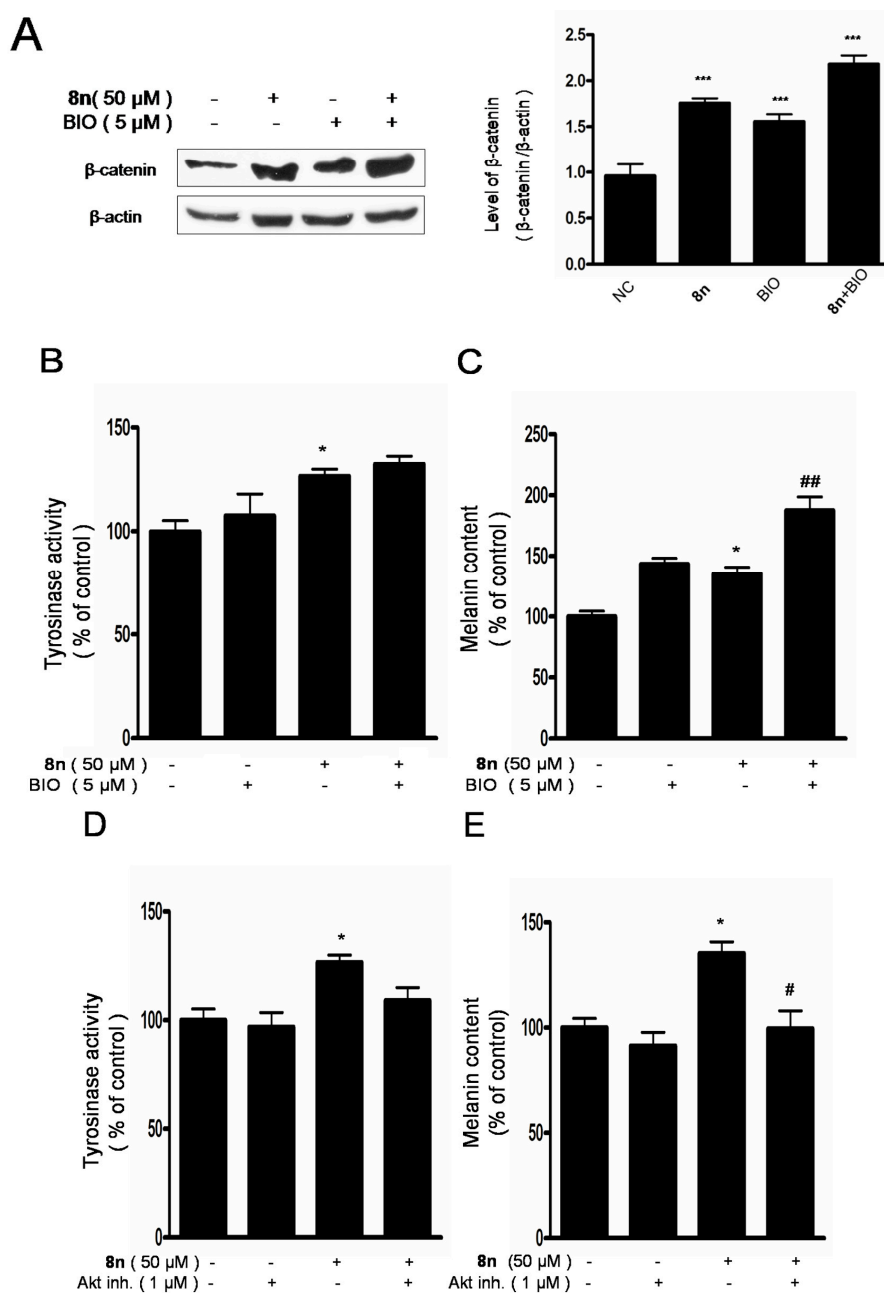


Figure 10. (A) β -catenin was detected in B16 cells pre-treated with or without BIO (5 μ M) and incubated with 8n (50 μ M) or not. (B–E) Inhibitors (BIO 5 μ M, Akt inhibitor IV 1 μ M) were pre-incubated with B16 cells for 2 h before addition of 8n at 50 μ M, followed by an additional incubation for 24 h or 48 h for tyrosinase activity and melanin content, respectively. * $p < 0.05$ compared with control; # $p < 0.05$, ## $p < 0.01$ as compared with 8n stimulation. “-” means pre-treated without 8n or Bio or Akt; “+” means pre-treated with 8n or Bio or Akt.

Currently, there are numerous reports about the close relationship between PI3K/Akt (phosphatidylinositol 3-kinases/protein kinase B) signal pathway and GSK3 β [42–46]. Activated Akt can phosphorylate GSK3 β resulting in inactivating GSK3 β and inhibit the degradation

of β -catenin [47]. Our data indicated that content of p-Akt and p-GSK3 β increased in B16 cells in the presence of **8n** after 48 h (Figure 9A). However, co-treatment with Akt inhibitor IV (5-(2-benzothiazolyl)-3-ethyl-2-[2-(methylphenylamino)ethenyl]-1-phenyl-1*H*-benzimidazolium iodide, a selective inhibitor of Akt that decreased the phosphorylation level of Akt and inhibited PI3K/Akt signal pathway [48]) distinctly aborted **8n**-mediated tyrosinase activity and melanin content (Figure 10D,E).

These results suggested that **8n** exerts a pigmented effect through the activation Wnt/ β -catenin signaling pathway by regulating Akt signal molecule.

The results of the present study indicated that 50 μ M of **8n** was more effective than the melanogenesis agent (8-MOP) since it increased melanin content (Figure 7A) and tyrosinase activity better than the latter (Figure 7B). In addition, the compound significantly up-regulated the level of MITF, and its related proteins, including TYR, TRP1, and TRP2, in a dose-dependent manner. Taken together, these findings suggested that **8n** was an effective tyrosinase activator to promote the melanin production in B16 cells.

According to the literature, the Wnt signalling pathway played a pivotal role in melanogenesis. By phosphatidylinositol-3-kinase (PI3K)/Akt activation and GSK3 β phosphorylation, MITF binded to the M-box of the tyrosinase promoter, thereby up-regulated melanogenic protein expression and induced melanogenesis [49–51]. Western blot analysis proved **8n** could activate the phosphorylation of Akt and GSK-3 β , indicating that it raised MITF transactivation of tyrosinase through GSK-3 β , which was similarly as mentioned in previous study [52]. Moreover, it was found that pretreatment with BIO enhanced **8n**-induced melanin production and tyrosinase activation (Figure 10B,C) when the up-regulation of melanin synthesis by the compound regulated by Akt/GSK3 β / β -catenin signaling was confirmed. However, co-treatment with Akt inhibitor IV significantly reversed these results (Figure 10D,E). Thus, Melanin production mediated by compound **8n** was probably triggered through both Akt and Wnt pathways, consistent with reports revealing that activation of Akt/GSK3 β / β -catenin influenced melanin production in B16 melanoma cells [53].

3. Materials and Methods

3.1. Chemistry

Reagents and solvents were purchased from Sigma (Shanghai, China), and used without further purification. Thin-layer chromatography (TLC) was carried out on glass plates coated with silica gel (Qingdao Haiyang Chemical Co., Qingdao, China, G60_{F-254}) and visualized by UV light (254 nm). The products were purified by column chromatography over silica gel (Qingdao Haiyang Chemical Co., 200–300 mesh). Melting points were determined on a Buchi B-540 apparatus and uncorrected. All of the NMR (nuclear magnetic resonance) spectra were recorded with a Varian400, 600 MHz NMR spectrometer in CDCl₃, using TMS (tetramethylsilane) as an internal standard. High-resolution mass spectra (HRMS) were recorded on AB SCIEX QSTAR Elite quadrupole time-of-flight mass spectrometry. The IR (infrared spectroscopy) data were recorded on a Thermo Fisher Scientific Nilolet 6700 FT-IR infrared spectrometer (KBr).

3.1.1. Preparation of 4-Methylumbelliferone (1)

To an ice-cold solution of resorcinol (2.0 g, 18.2 mol) in dioxane, conc. H₂SO₄ (0.5 mL) was added dropwise under 20 °C. After the addition of conc. H₂SO₄, ethyl acetoacetate (2.8 g, 21.8 mmol) was added, and the mixture was heated to 60 °C for 4 h. Then, the mixture was poured into cold water, and the precipitate was filtered and dried under reduced pressure. The resulting mixture was recrystallized from methanol to give compound as white needle crystals. Yield 92%, m.p. 202–204 °C.

3.1.2. Preparation of 7-(2-Hydroxyethoxy)-4-methyl-2H-chromen-2-one (2)

A mixture of **1** (0.88 g, 5.0 mmol) with chloroethanol (0.60 g, 7.5 mmol) and anhydrous K_2CO_3 (1.4 g, 10 mmol) in acetone (50 mL) was refluxed under stirring for 4 h. After cooling, the reaction mixture was filtered, and the filtrate was evaporated under reduced pressure. The obtained residue was purified by silica gel chromatography with petroleum ether/ethylacetate or chloroform to give intermediate **3**. Yield 95%, white solid, m.p. 108–110 °C; 1H NMR (400 MHz, $CDCl_3$) δ 7.51 (d, $J = 9.0$ Hz, 1H), 6.91–6.83 (m, 2H), 6.15 (d, $J = 1.1$ Hz, 1H), 4.15 (t, $J = 8.7$ Hz, 2H), 4.01 (m, 2H), 2.40 (d, $J = 1.1$ Hz, 3H).

3.1.3. Preparation of 7-(2-Oxoethoxy)-4-methyl-2H-chromen-2-one (3)

A solution of oxalyl chloride (0.252 g, 2 mmol) in anhydrous CH_2Cl_2 (5 mL) was cooled to -78 °C under a nitrogen atmosphere, and a solution of DMSO (0.156 g, 2 mmol) in CH_2Cl_2 (2 mL) was added dropwise (the temperature was kept below -65 °C), and stirred for 10 min. A solution of alcohol **2** (0.22 g, 1 mmol) in CH_2Cl_2 (15 mL) was added dropwise at a temperature below -65 °C and stirred for another 30 min. Triethylamine (0.505 g, 5 mmol) was then added dropwise. The reaction mixture was stirred for 15 min at a temperature below -65 °C and allowed to warm up to room temperature. The reaction mixture was diluted with CH_2Cl_2 and was filtered through a pad of silica gel. Removal of the solvent under vacuum afforded the aldehydes **3**. Yield 97%, white solid, m.p. 140–142 °C; 1H NMR (400 MHz, $CDCl_3$) δ 9.85 (s, 1H), 7.53 (d, $J = 8.8$ Hz, 1H), 6.89 (dd, $J = 8.8, 2.6$ Hz, 1H), 6.78 (d, $J = 2.5$ Hz, 1H), 6.15 (d, $J = 1.0$ Hz, 1H), 4.68 (s, 2H), 2.39 (d, $J = 0.9$ Hz, 3H).

3.1.4. Preparation of Compounds 4

A solution of aldehydes **3** (0.5 mmol) in H_2O -dioxane (1:1, 3 mL) was added dropwise to a refluxing aqueous solution of NaOH (1.0 M, 10 mL) under stirring for more than 30 min. The resulted mixture was stirred at reflux for an additional 4 h and then cooled down to room temperature. The solution was acidified to pH = 3 with 85% phosphoric acid and was left overnight. The resultant mixture was extracted with ethylacetate three times. The organic phase was then washed with brine and dried over anhydrous Na_2SO_4 . After removal of the solvents, the residue was purified by flash chromatography on silica gel eluted with $V_{\text{petroleum ether}}:V_{\text{ethylacetate}} = 1:10$ to afford a pair of isomer.

5-Methyl-7H-furo[3,2-g]chromen-7-one (**4a**). Yield 73%, white solid, m.p. 160–162 °C; 1H NMR (400 MHz, $CDCl_3$) δ 7.81 (s, 1H), 7.69 (d, $J = 2.2$ Hz, 1H), 7.47 (s, 1H), 6.85 (d, $J = 2.1$ Hz, 1H), 6.27 (s, 1H), 2.50 (s, 3H). ^{13}C NMR (101 MHz, $CDCl_3$) δ 161.24, 156.43, 152.78, 151.75, 146.96, 124.77, 116.70, 113.62, 106.67, 100.00, 19.30; IR (KBr) ν : 2921, 1723, 1630, 1385, 1137, 1031, 928 cm^{-1} ; HRMS (ESI) calcd for $C_{12}H_9O_3[M + H]^+$ 201.0552, found 201.0540.

4-Methyl-2H-furo[2,3-h]chromen-2-one (**4b**). Yield 11%, white solid, m.p. 119–120 °C; 1H NMR (400 MHz, $CDCl_3$) δ 7.69 (d, $J = 2.2$ Hz, 1H), 7.53 (d, $J = 8.8$ Hz, 1H), 7.45 (d, $J = 8.7$ Hz, 1H), 7.15 (d, $J = 2.1$ Hz, 1H), 6.28 (s, 1H), 2.51 (s, 3H). ^{13}C NMR (101 MHz, $CDCl_3$) δ 160.89, 157.25, 153.58, 145.76, 120.48, 117.00, 112.86, 110.02, 108.41, 104.37, 19.44; IR (KBr) ν : 2919, 1718, 1617, 1264, 1065, 761 cm^{-1} ; HRMS (ESI) calcd for $C_{12}H_9O_3[M + H]^+$ 201.0552, found 201.0559.

3.1.5. Preparation of 7-Oxo-7H-furo[3,2-g]chromene-5-carbaldehyde (5)

Powdered SeO_2 (3.33 g, 30 mmol) was added to a solution of **4a** (8.0 g, 20 mmol) in 20 mL of hot dry xylene and the mixture were refluxed for 12 h with vigorous stirring under nitrogen. The reaction mixture was filtered to remove black Se, and the deep orange filtrate was allowed to stand overnight. Almost pure crystals of **5** could be separated from the solution. Yield 63%, yellow solid, m.p. 178–180 °C; 1H NMR (400 MHz, $CDCl_3$) δ 10.14 (s, 1H), 8.90 (s, 1H), 7.72 (d, $J = 2.1$ Hz, 1H), 7.54 (s, 1H), 6.89 (d, $J = 2.0$ Hz, 1H), 6.86 (s, 1H).

3.1.6. Preparation of 5-(Hydroxymethyl)-7*H*-furo[3,2-*g*]chromen-7-one (6)

Compound 5 (4.28 g, 20 mmol) was dissolved in ethanol (130 mL), sodium borohydride (380 mg, 10.0 mmol) was added, and the solution was stirred for 2 h at room temperature. Thereafter the suspension was carefully hydrolyzed with 1M HCl (20 mL), diluted with H₂O and extracted three times with CH₂Cl₂. The organic phase was washed with brine, dried over Na₂SO₄, and then evaporated under reduced pressure. The residue was purified by flash chromatography on silica gel eluted with $V_{\text{chloroform}}:V_{\text{methanol}} = 30:1$ to afford alcohol 7. Yield 76%, white solid, m.p. 204–206 °C; ¹H NMR (400 MHz, CDCl₃) ¹H NMR (600 MHz, CD₃OD) δ 7.95 (s, 1H), 7.87 (d, *J* = 1.9 Hz, 1H), 7.55 (s, 1H), 6.97 (d, *J* = 2.0 Hz, 1H), 6.56 (s, 1H), 4.94 (s, 2H). ¹³C NMR (101 MHz, CD₃OD) δ 163.57, 158.32, 152.82, 148.71, 129.23, 127.39, 117.21, 115.30, 110.23, 107.75, 100.51, 61.09.

3.1.7. Preparation of (7-Oxo-7*H*-furo[3,2-*g*]chromen-5-yl)methyl acetate (7)

A mixture of 7 (0.022 g, 0.09 mmol), 4-dimethylaminopyridine DMAP (1 mg), and one drop of acetic anhydride in 2 mL of anhydrous pyridine was stirred at room temperature overnight under nitrogen atmosphere, 5 mL of icy water was then added. The reaction mixture was extracted with ethyl acetate three times, and the organic layer was washed with brine and dried over anhydrous Na₂SO₄. After the removal of solvent, the crude product was purified by flash column chromatography over silica gel eluted with $V_{\text{petroleumether}}/V_{\text{ethylacetate}} = 3:1$ to give acetate 7. Yield 80%, white solid, m.p. 198–200 °C; ¹H NMR (400 MHz, CDCl₃) δ 7.82 (s, 1H), 7.71 (d, *J* = 2.1 Hz, 1H), 7.47 (s, 1H), 6.86 (d, *J* = 2.0 Hz, 1H), 6.49 (s, 1H), 5.37 (s, 2H), 2.23 (s, 3H).

3.1.8. General Procedure Of preparation of Esters 8a–8p

1,3-Dicyclohexylcarbodiimide (DCC, 0.82 g, 4 mmol) was added to a solution of 7 (0.86 g, 4 mmol), different benzoic acid (5 mmol) and DMAP (0.49 g, 4 mmol) in dry CH₂Cl₂ (25 mL) at 0 °C under nitrogen. After 10 min at 0 °C, the mixture was stirred at room temperature for 12 h. After filtration, the organic filtrate was washed with 1.2 M hydrochloric acid, saturated aqueous sodium hydrogen carbonate, then dried over sodium sulfate and evaporated under reduced pressure. The residue was purified by flash chromatography on silica gel eluted with petroleum ether/ethyl acetate to give corresponding benzoate 8a–8p.

(7-Oxo-7*H*-furo[3,2-*g*]chromen-5-yl)methyl-4-methylbenzoate (8a). Yield 81%, white solid, m.p. 181–182 °C; ¹H NMR (600 MHz, CDCl₃) δ 8.02 (d, *J* = 8.1 Hz, 2H), 7.81 (s, 1H), 7.71 (d, *J* = 2.1 Hz, 1H), 7.53 (s, 1H), 7.29 (d, *J* = 8.0 Hz, 2H), 6.86 (d, *J* = 2.1 Hz, 1H), 6.60 (s, 1H), 5.60 (s, 2H), 2.44 (s, 3H). ¹³C NMR (101 MHz, CDCl₃) δ 165.77, 160.75, 156.37, 151.71, 149.62, 147.14, 144.67, 129.89, 129.40, 126.23, 124.94, 115.46, 113.68, 111.57, 106.57, 100.37, 61.65, 21.76; IR (KBr) *v*: 2925, 1717, 1634, 1576, 1447, 1278, 1264, 1156, 1135, 874, 750 cm⁻¹; HRMS (ESI) calcd for C₂₀H₁₅O₅[M + H]⁺ 335.0914, found 335.0931.

(7-Oxo-7*H*-furo[3,2-*g*]chromen-5-yl)methyl-2-methylbenzoate (8b). Yield 84%, white solid, m.p. 169–171 °C; ¹H NMR (400 MHz, CDCl₃) δ 8.04 (dd, *J* = 7.8, 0.8 Hz, 1H), 7.83 (s, 1H), 7.72 (d, *J* = 2.1 Hz, 1H), 7.54 (s, 1H), 7.50–7.44 (m, 1H), 7.33–7.28 (m, 2H), 6.87 (d, *J* = 2.2 Hz, 1H), 6.59 (s, 1H), 5.60 (s, 2H), 2.65 (s, 3H). ¹³C NMR (101 MHz, CDCl₃) δ 166.28, 160.68, 156.35, 151.71, 149.55, 147.11, 141.04, 132.82, 132.00, 130.76, 125.99, 124.91, 115.45, 113.69, 111.74, 106.53, 100.36, 61.61, 21.88; IR (KBr) *v*: 2926, 1723, 1632, 1577, 1449, 1278, 1263, 1155, 1135, 873, 749 cm⁻¹; HRMS (ESI) calcd for C₂₀H₁₅O₅[M + H]⁺ 335.0914, found 335.0944.

(7-Oxo-7*H*-furo[3,2-*g*]chromen-5-yl)methyl-4-methoxybenzoate (8c). Yield 80%, white solid, m.p. 155–157 °C; ¹H NMR (400 MHz, CDCl₃) δ 8.09 (d, *J* = 8.8 Hz, 2H), 7.82 (s, 1H), 7.71 (d, *J* = 2.1 Hz, 1H), 7.54 (s, 1H), 6.97 (d, *J* = 8.9 Hz, 2H), 6.86 (d, *J* = 2.0 Hz, 1H), 6.59 (s, 1H), 5.60 (s, 2H), 3.89 (s, 3H). ¹³C NMR (101 MHz, CDCl₃) δ 165.56, 160.91, 156.52, 151.87, 149.90, 147.28, 132.12, 129.20, 125.08, 121.44, 115.62, 114.11, 113.91, 111.67, 106.72, 100.51, 61.68, 55.69; IR (KBr) *v*: 2927, 1724, 1634, 1575, 1448, 1277, 1265, 1156, 1134, 872, 748 cm⁻¹; HRMS (ESI) calcd for C₂₀H₁₅O₆[M + H]⁺ 351.0863, found 351.0855.

(7-Oxo-7H-furo[3,2-g]chromen-5-yl)methyl-2-methoxybenzoate (**8d**). Yield 82%, white solid, m.p. 148–149 °C; ^1H NMR (400 MHz, CDCl_3) δ 7.92 (dd, $J = 7.9, 1.8$ Hz, 1H), 7.82 (s, 1H), 7.71 (d, $J = 2.2$ Hz, 1H), 7.57–7.50 (m, 1H), 7.06–7.00 (m, 2H), 6.86 (d, $J = 2.2$ Hz, 1H), 6.73 (s, 1H), 5.60 (s, 2H), 3.95 (s, 3H). ^{13}C NMR (101 MHz, CDCl_3) δ 165.56, 160.86, 159.54, 156.33, 151.72, 149.65, 147.10, 134.49, 132.20, 124.87, 120.35, 118.61, 115.50, 113.73, 112.11, 111.79, 106.57, 100.30, 61.78, 55.94; IR (KBr) ν : 2927, 1718, 1633, 1576, 1450, 1279, 1264, 1157, 1136, 873, 760, 750 cm^{-1} ; HRMS (ESI) calcd for $\text{C}_{20}\text{H}_{15}\text{O}_6[\text{M} + \text{H}]^+$ 351.0863, found 351.0839.

(7-Oxo-7H-furo[3,2-g]chromen-5-yl)methyl-4-chlorobenzoate (**8e**). Yield 78%, light yellow solid, m.p. 201–202 °C; ^1H NMR (400 MHz, CDCl_3) δ 8.07 (d, $J = 8.6$ Hz, 2H), 7.80 (s, 1H), 7.72 (d, $J = 2.3$ Hz, 1H), 7.55 (s, 1H), 7.48 (d, $J = 8.6$ Hz, 2H), 6.87 (d, $J = 2.1$ Hz, 1H), 6.57 (s, 1H), 5.62 (s, 2H). ^{13}C NMR (101 MHz, CDCl_3) δ 164.89, 160.63, 156.42, 151.72, 149.20, 147.22, 140.40, 131.23, 129.10, 127.41, 125.00, 115.41, 113.58, 111.72, 106.56, 100.46, 62.03; IR (KBr) ν : 1717, 1624, 1574, 1541, 1457, 1270, 1243, 1129, 1090, 669 cm^{-1} ; HRMS (ESI) calcd for $\text{C}_{19}\text{H}_{12}\text{ClO}_5[\text{M} + \text{H}]^+$ 355.0368, found 355.0390.

(7-Oxo-7H-furo[3,2-g]chromen-5-yl)methyl-2-chlorobenzoate (**8f**). Yield 75%, light yellow solid, m.p. 183–185 °C; ^1H NMR (400 MHz, CDCl_3) δ 7.95 (dd, $J = 7.6, 1.3$ Hz, 1H), 7.82 (s, 1H), 7.72 (d, $J = 2.3$ Hz, 1H), 7.54 (s, 1H), 7.53–7.48 (m, 2H), 7.41–7.35 (m, 1H), 6.87 (d, $J = 2.2$ Hz, 1H), 6.64 (s, 1H), 5.63 (s, 2H). ^{13}C NMR (101 MHz, CDCl_3) δ 164.92, 160.79, 156.55, 151.89, 149.04, 147.33, 134.37, 133.55, 131.94, 131.60, 128.88, 127.01, 125.11, 115.68, 113.74, 112.24, 106.71, 100.56, 62.57; IR (KBr) ν : 1734, 1707, 1635, 1577, 1450, 1412, 1240, 1156, 1113, 1028, 746 cm^{-1} ; HRMS (ESI) calcd for $\text{C}_{19}\text{H}_{12}\text{ClO}_5[\text{M} + \text{H}]^+$ 355.0368, found 355.0387.

(7-Oxo-7H-furo[3,2-g]chromen-5-yl)methyl-3,4-dichlorobenzoate (**8g**). Yield 70%, light yellow solid, m.p. 198–200 °C; ^1H NMR (400 MHz, CDCl_3) δ 8.20 (d, $J = 2.0$ Hz, 1H), 7.95 (dd, $J = 8.4, 1.9$ Hz, 1H), 7.80 (s, 1H), 7.73 (d, $J = 2.3$ Hz, 1H), 7.59 (d, $J = 8.4$ Hz, 1H), 7.55 (s, 1H), 6.87 (d, $J = 2.1$ Hz, 1H), 6.55 (s, 1H), 5.63 (s, 2H). ^{13}C NMR (101 MHz, CDCl_3) δ 163.97, 160.54, 158.21, 153.31, 147.28, 143.32, 138.63, 136.04, 131.73, 130.90, 128.83, 127.59, 122.64, 120.23, 115.41, 111.86, 106.56, 100.50, 62.34; IR (KBr) ν : 1716, 1633, 1620, 1568, 1513, 1447, 1361, 1250, 1089, 748 cm^{-1} ; HRMS (ESI) calcd for $\text{C}_{19}\text{H}_{11}\text{Cl}_2\text{O}_5[\text{M} + \text{H}]^+$ 388.9978, found 388.9955.

(7-Oxo-7H-furo[3,2-g]chromen-5-yl)methyl-3,5-dichlorobenzoate (**8h**). Yield 71%, light yellow solid, m.p. 223–224 °C; ^1H NMR (400 MHz, CDCl_3) δ 7.98 (d, $J = 1.9$ Hz, 2H), 7.79 (s, 1H), 7.73 (d, $J = 2.2$ Hz, 1H), 7.62 (t, $J = 1.9$ Hz, 1H), 7.55 (s, 1H), 6.87 (d, $J = 2.1$ Hz, 1H), 6.54 (s, 1H), 5.63 (s, 2H). ^{13}C NMR (101 MHz, CDCl_3) δ 163.67, 160.63, 156.59, 151.86, 148.84, 147.41, 135.83, 133.77, 131.88, 128.96, 128.32, 125.18, 115.52, 112.04, 106.68, 100.63, 62.64; IR (KBr) ν : 1718, 1636, 1571, 1451, 1261, 1156, 1130, 870, 748 cm^{-1} ; HRMS (ESI) calcd for $\text{C}_{19}\text{H}_{11}\text{Cl}_2\text{O}_5[\text{M} + \text{H}]^+$ 388.9978, found 388.9967.

(7-Oxo-7H-furo[3,2-g]chromen-5-yl)methyl-4-fluorobenzoate (**8i**). Yield 83%, off-white solid, m.p. 177–178 °C; ^1H NMR (400 MHz, CDCl_3) δ 8.19–8.12 (m, 2H), 7.81 (s, 1H), 7.72 (d, $J = 2.2$ Hz, 1H), 7.54 (s, 1H), 7.18 (t, $J = 8.6$ Hz, 2H), 6.87 (d, $J = 2.1$ Hz, 1H), 6.57 (s, 1H), 5.62 (s, 2H). ^{13}C NMR (101 MHz, CDCl_3) δ 164.87, 160.78, 156.54, 151.85, 149.47, 147.35, 146.81, 132.62, 125.13, 116.20, 115.98, 115.56, 111.78, 106.69, 100.56, 62.04; IR (KBr) ν : 1716, 1604, 1508, 1456, 1265, 1237, 1154, 849, 743 cm^{-1} ; HRMS (ESI) calcd for $\text{C}_{19}\text{H}_{12}\text{FO}_5[\text{M} + \text{H}]^+$ 339.0663, found 339.0689.

(7-Oxo-7H-furo[3,2-g]chromen-5-yl)methyl-2,4-difluorobenzoate (**8j**). Yield 77%, off-white solid, m.p. 185–186 °C; ^1H NMR (400 MHz, CDCl_3) δ 8.08 (td, $J = 8.5, 6.5$ Hz, 1H), 7.81 (s, 1H), 7.72 (d, $J = 2.2$ Hz, 1H), 7.54 (s, 1H), 7.04–6.90 (m, 2H), 6.87 (d, $J = 2.0$ Hz, 1H), 6.63 (s, 1H), 5.63 (s, 2H). ^{13}C NMR (101 MHz, CDCl_3) δ 165.18, 164.55, 162.94, 160.79, 156.54, 151.85, 149.00, 147.33, 134.41, 125.10, 115.56, 113.67, 112.34, 112.12, 111.97, 106.70, 105.76, 100.56, 62.40; IR (KBr) ν : 1718, 1615, 1507, 1452, 1259, 1125, 1090, 852, 747 cm^{-1} ; HRMS (ESI) calcd for $\text{C}_{19}\text{H}_{11}\text{F}_2\text{O}_5[\text{M} + \text{H}]^+$ 357.0569, found 339.0545.

(7-Oxo-7H-furo[3,2-g]chromen-5-yl)methyl-benzoate (**8k**). Yield 85%, off-white solid, m.p. 213–215 °C; ^1H NMR (400 MHz, CDCl_3) δ 8.16–8.11 (m, 2H), 7.82 (s, 1H), 7.72 (d, $J = 2.2$ Hz, 1H), 7.64 (t, $J = 7.4$ Hz,

1H), 7.56–7.47 (m, 3H), 6.87 (d, $J = 2.2$ Hz, 1H), 6.61 (s, 1H), 5.63 (s, 2H). ^{13}C NMR (101 MHz, CDCl_3) δ 165.87, 160.85, 156.54, 151.88, 149.61, 147.32, 133.94, 131.04, 130.01, 128.85, 125.11, 115.60, 113.81, 111.79, 106.72, 100.55, 61.96; IR (KBr) ν : 1717, 1635, 1506, 1451, 1268, 1158, 1116, 1094, 847, 745 cm^{-1} ; HRMS (ESI) calcd for $\text{C}_{19}\text{H}_{13}\text{O}_5[\text{M} + \text{H}]^+$ 321.0757, found 321.0760.

(7-Oxo-7H-furo[3,2-g]chromen-5-yl)methyl-4-nitrobenzoate (**8l**). Yield 70%, off-white solid, m.p. 201–203 °C; ^1H NMR (400 MHz, CDCl_3) δ 8.38–8.26 (m, 5H), 7.81 (s, 1H), 7.73 (d, $J = 2.3$ Hz, 1H), 7.56 (s, 1H), 6.87 (d, $J = 2.1$ Hz, 1H), 6.57 (s, 1H), 5.68 (s, 2H). ^{13}C NMR (101 MHz, CDCl_3) δ 164.07, 156.71, 151.89, 149.63, 148.77, 147.48, 135.63, 131.18, 129.03, 126.84, 124.01, 115.49, 114.44, 112.12, 106.68, 100.72, 62.78; IR (KBr) ν : 1720, 1624, 1577, 1527, 1451, 1270, 1244, 1089 cm^{-1} ; HRMS (ESI) calcd for $\text{C}_{19}\text{H}_{12}\text{NO}_7[\text{M} + \text{H}]^+$ 366.0608, found 366.0586.

(7-Oxo-7H-furo[3,2-g]chromen-5-yl)methyl-4-(trifluoromethyl)benzoate (**8m**). Yield 66%, off-white solid, m.p. 219–220 °C; ^1H NMR (400 MHz, CDCl_3) δ 8.25 (d, $J = 8.0$ Hz, 2H), 7.81 (s, 1H), 7.77 (d, $J = 8.3$ Hz, 2H), 7.73 (d, $J = 2.3$ Hz, 1H), 7.56 (s, 1H), 6.87 (d, $J = 2.2$ Hz, 1H), 6.58 (s, 1H), 5.66 (s, 2H). ^{13}C NMR (101 MHz, CDCl_3) δ 166.84, 160.71, 156.60, 151.87, 149.06, 147.42, 137.47, 130.44, 127.12, 125.94, 125.18, 115.53, 112.03, 110.18, 106.70, 100.67, 62.48; IR (KBr) ν : 1734, 1718, 1625, 1578, 1559, 1326, 1271, 1131 cm^{-1} ; HRMS (ESI) calcd for $\text{C}_{20}\text{H}_{12}\text{F}_3\text{O}_5[\text{M} + \text{H}]^+$ 389.0631, found 389.0642.

(7-Oxo-7H-furo[3,2-g]chromen-5-yl)methyl-3-nitrobenzoate (**8n**). Yield 68%, off-white solid, m.p. 202–204 °C; ^1H NMR (400 MHz, CDCl_3) δ 8.52–8.37 (m, 4H), 7.83 (s, 1H), 7.73 (d, $J = 2.2$ Hz, 1H), 7.56 (s, 1H), 6.88 (d, $J = 2.1$ Hz, 1H), 6.56 (s, 1H), 5.69 (s, 2H). ^{13}C NMR (101 MHz, CDCl_3) δ 164.82, 162.22, 156.99, 156.59, 147.46, 142.58, 135.51, 133.05, 130.20, 129.53, 128.34, 125.05, 115.55, 112.20, 109.31, 106.70, 100.71, 62.77; IR (KBr) ν : 1733, 1719, 1624, 1576, 1532, 1351, 1270, 1087 cm^{-1} ; HRMS (ESI) calcd for $\text{C}_{19}\text{H}_{12}\text{NO}_7[\text{M} + \text{H}]^+$ 366.0608, found 366.0633.

(7-Oxo-7H-furo[3,2-g]chromen-5-yl)methyl-3,5-dinitrobenzoate (**8o**). Yield 52%, off-white solid, m.p. 210–211 °C; ^1H NMR (400 MHz, CDCl_3) δ 9.29 (d, $J = 1.9$ Hz, 1H), 9.23 (d, $J = 2.0$ Hz, 1H), 7.83 (s, 1H), 7.74 (d, $J = 2.2$ Hz, 1H), 7.57 (s, 1H), 6.89 (d, $J = 2.1$ Hz, 1H), 6.53 (s, 1H), 5.75 (s, 2H). ^{13}C NMR (101 MHz, CDCl_3) δ 165.43, 161.06, 156.74, 152.15, 148.91, 146.64, 144.84, 135.53, 132.04, 129.76, 128.71, 124.84, 116.13, 112.15, 107.32, 100.31, 62.46; IR (KBr) ν : 1718, 1623, 1575, 1540, 1436, 1311, 1243, 1089 cm^{-1} ; HRMS (ESI) calcd for $\text{C}_{19}\text{H}_{11}\text{N}_2\text{O}_9[\text{M} + \text{H}]^+$ 411.0459, found 411.0476.

(7-Oxo-7H-furo[3,2-g]chromen-5-yl)methyl-2-iodobenzoate (**8p**). Yield 78%, yellow solid, m.p. 186–187 °C; ^1H NMR (400 MHz, CDCl_3) δ 8.06 (d, $J = 8.0$ Hz, 1H), 7.92 (d, $J = 7.6$ Hz, 1H), 7.82 (s, 1H), 7.72 (d, $J = 1.9$ Hz, 1H), 7.54 (s, 1H), 7.50–7.42 (m, 2H), 6.87 (d, $J = 2.0$ Hz, 1H), 6.62 (s, 1H), 5.63 (s, 2H). ^{13}C NMR (101 MHz, CDCl_3) δ 160.79, 156.46, 149.03, 147.35, 141.89, 133.56, 131.41, 128.33, 125.13, 123.26, 116.70, 115.69, 113.65, 112.28, 110.17, 106.72, 100.58, 62.59; IR (KBr) ν : 1735, 1705, 1636, 1564, 1516, 1441, 1230, 1282, 1149, 1123, 748 cm^{-1} ; HRMS (ESI) calcd for $\text{C}_{19}\text{H}_{12}\text{IO}_5[\text{M} + \text{H}]^+$ 446.9724, found 446.9741.

3.2. Biological Activity

Akt (also named PKB, protein kinase B), p-Akt (Ser308), GSK3 β , p-GSK3 β (Ser9), and β -actin antibodies were purchased from Cell Signaling Technology (Danvers, MA, USA). β -catenin, p- β -catenin (Ser33), antibodies against TYR, TRP1, and TRP2 were bought from Santa Cruz Technology (Dallas, TX, USA). Anti-MITF antibody was purchased from Millipore (Billerica, MA, USA). Anti-mouse, anti-goat and anti-rabbit IgG antibodies (horseradish peroxidase conjugated) were purchased from Santa Cruz Biotechnology (Dallas, TX, USA).

Dimethylsulfoxide (DMSO) was bought from Sigma (St. Louis, MO, USA), [2-(2-methoxy-4-nitrophenyl)-3-(4-nitrophenyl)-5-(2,4-disulfophenyl)-2H-tetrazolium] (CCK-8) was purchased from Trans Gen Biotechnology (Beijing, China). Nuclear and cytoplasmic protein extraction kit was bought from Beyotime Biotechnology, (Shanghai, China). Akt inhibitor IV was bought from EMD Biosciences, (La Jolla, CA, USA). BIO was purchased from AMQUAR Biology, (Shanghai, China).

3.2.1. Cell Cultures

The murine B16 melanoma cell line was purchased from Chinese Academy of Sciences (Beijing, China). The cells were maintained in Dulbecco's modified Eagle's medium (DMEM, Gibco Life Technologies, Paris, France), supplemented with 10% (*v/v*) FBS, penicillin G (100 U/mL), and streptomycin (100 mg/mL) (Gibco-BRL, Grand Island, NY, USA) in 5% CO₂ at 37 °C.

3.2.2. Cell Morphology and Cell Viability Measurement

Cell morphology was examined under a LEICA DMI8 microscope (LEICA microsystems CMS GmbH, Wetzlar, Germany). The cell viability was assayed by adding CCK-8 solution. Generally speaking, The B16 cells were seeded in 96-well plates at a density of 1×10^4 cells per well and were allowed to adhere for 24 h. The medium was replaced with medium containing **8n** diluted to the appropriate concentrations. The control cells were treated with DMSO at a final concentration of 0.1%. After 48 h, the culture medium of the cells was discarded, 10 µL of CCK-8 solution was added into each well and cells were incubated at 37 °C for another 2 h. The absorbance was measured at 450 nm using a Spectra Max M5 (Molecular Devices, San Jose, CA, USA). All of the assays were performed in triplicate. Absorbance of cells without treatment was regarded as 100% of cell survival. Cell viability was calculated using the following formula: cell viability (%) = $(A_{\text{sample}}/A_{\text{control}}) \times 100\%$.

3.2.3. Melanin Measurement

B16 cells were seeded at a density of 2×10^5 cells/well in a 6-well plate. After overnight incubation, test samples were added to individual wells, cells were incubated for 48 h, and were washed twice with ice-cold PBS (phosphate buffered solution). After cells lysed, the harvested cells were centrifuged, and the pellet was dissolved by adding 1 N NaOH, followed by incubation at 80 °C for 1 h. Each lysate (150 µL) was put in a 96-well microplate, and measured spectro-photometrically at 405 nm by a multi-plate reader. Protein concentration of each sample was determined by BCA Protein Assay Kit (Biomed, Beijing, China). Intracellular melanin amount was expressed as abs/µg protein was shown as a percentage value. The percentage value of the **8n**-treated cells was calculated with respect to the untreated cells.

3.2.4. Tyrosinase Activity Assay

The assay for tyrosinase activity was carried out, as previously described [54], with a slight modification. B16 cells were seeded in a 6-well plate at a density of 2×10^5 cells per well and allowed to attach for 24 h. Test samples were then added to individual wells. After a 24 h incubation, cells were washed with ice-cold PBS twice, lysed with 1% Triton X-100 solution containing 1% sodium deoxycholate for 30 min at −80 °C, each lysate was centrifuged at $12,000 \times g$ for 15 min to obtain the supernatant. After protein quantification and adjustment, 90 µL of the supernatant was incubated in duplicate with 10 µL of freshly prepared substrate solution (10 mM L-DOPA) in a well of a 96-well plate. Then the cells were incubated at 37 °C in dark for 60 min, the absorbance was measured at 490 nm and the **8n**-treated cells was presented as percentage against the untreated cells.

3.2.5. Western Blot Analysis

B16 cells were treated with different concentrations of **8n** in a 6-well plate for 48 h. Cells were then lysed in cold RIPA (radio immunoprecipitation assay) Lysis Buffer (pH 7.4) containing protease and protease inhibitor cocktail [1 M 4-nitrophenyl phosphate disodium salt hexahydrate (PNPP), 1 M sodium fluoride (NaF), 10mMphenylmethanesulfonylfluoride (PMSF), 100 mM benzamidine, 100 mM DL-Dithiothreitol (DTT), 200mM sodium orthovanadate (OV)] for 30 min on ice. The lysates were centrifuged at 12,000 rpm for 20 min at 4 °C before the supernatant was collected. The protein samples concentration was measured by BCA Protein Assay Kit (Biomed, Beijing, China) and was separated by 10% SDS polyacrylamide gels and transferred onto polyvinylidene fluoride (PVDF) membranes (Merck

Millipore Ltd., Billerica, MA, USA), Membranes were incubated with the primary antibodies at 4 °C overnight, and then incubated with horseradish peroxidase-conjugated secondary antibodies for 1 h at room temperature. The targeted proteins were detected by ECL western blotting detection reagents (GE Healthcare, Beijing, China), and were visualized using the ChemiDoc MP Imaging system (Bio-Rad Laboratories, Inc., Berkeley, CA, USA). All western bolt assay results were performed in triplicate.

3.2.6. Statistical Analysis

All data were expressed as the means \pm standard deviations and statistical analysis was performed by one-way ANOVA followed by Tukey post hoc test for multiple comparison tests. A *p* value of < 0.05 was considered a significant difference.

4. Conclusions

In summary, a series of ester furocoumarin derivatives had been prepared via total synthesis or structural modification. Half of compounds exhibited a better activity on melanin synthesis than positive control (8-MOP) in B16 melanoma cells. Among them, compounds **8n** (200%) and **8o** (197%) were nearly 1.5-fold stronger than 8-MOP (136%).

Western blot analysis showed that **8n** promoted phosphorylation of Akt, and thus probably increased the non-activated GSK3 β , which inhibits the phosphorylation of β -catenin and ceased its degradation via proteasome. The accumulation of β -catenin probably leads to the activation of transcription of MITF, TYR family, and thus the subsequent induction of melanin synthesis. These results indicated that **8n** stimulated melanin biosynthesis by up-regulation of MITF and TYR family via Akt/GSK3 β / β -catenin signaling pathways.

In the view of the widespread application of furocoumarins in vitiligo nowadays, similar structural modification on C-5 position may be beneficial to explore potential melanogenesis-modulating candidates. Signaling pathway research would shed light on the molecular function of furocoumarins in melanogenesis. Further studies in vivo on vitiligo model mice are under way to assess the safety and efficacy of **8n** for clinical use.

Acknowledgments: This work was supported by the Funds for the Xinjiang Key Research and Development Program (2016B03038-3); West Light Foundation of the Chinese Academy of Science (No. XBBS201403); Natural Science Foundation of Xinjiang, China (No. 2017D01A76).

Author Contributions: Chao Niu and Li Yin performed experiments. Chao Niu prepared the manuscript. Haji Akber Aisa designed the study and revised the paper. All authors read and reviewed the manuscript.

Conflicts of Interest: The authors declare no conflict of interest.

References

1. Ezzedine, K.; Sheth, V.; Rodrigues, M.; Eleftheriadou, V.; Harris, J.E.; Hamzavi, I.H.; Pandya, A.G. Vitiligo is not a cosmetic disease. *J. Am. Acad. Dermatol.* **2015**, *73*, 883–885. [[CrossRef](#)] [[PubMed](#)]
2. Halder, R.M.; Chappell, J.L. Vitiligo Update. *Semin. Cutan. Med. Surg.* **2009**, *28*, 86–92. [[CrossRef](#)] [[PubMed](#)]
3. Namazi, M.R. Neurogenic dysregulation, oxidative stress, autoimmunity, and melanocytorrhagy in vitiligo: Can they be interconnected? *Pigment Cell Res.* **2007**, *20*, 360–363. [[CrossRef](#)] [[PubMed](#)]
4. Ralf Paus, L.; Schallreuter, K.U.; Bahadoran, P.; Picardo, M.; Slominski, A.; Ellassiuty, Y.E.; Kemp, E.H.; Giachino, C.; Liu, J.B.; Luiten, R.M.; et al. Vitiligo pathogenesis: Autoimmune disease, genetic defect, excessive reactive oxygen species, calcium imbalance, or what else? *Exp. Dermatol.* **2008**, *17*, 139–140. [[CrossRef](#)]
5. Schallreuter, K.U.; Kothari, S.; Chavan, B.; Spencer, J.D. Regulation of melanogenesis—Controversies and new concepts. *Exp. Dermatol.* **2008**, *17*, 395–404. [[CrossRef](#)] [[PubMed](#)]
6. Sandoval-Cruz, M.; García-Carrasco, M.; Sánchez-Porrás, R.; Mendoza-Pinto, C.; Jiménez-Hernández, M.; Munguía-Realpozo, P.; Ruiz-Argüelles, A. Immunopathogenesis of vitiligo. *Autoimmun. Rev.* **2011**, *10*, 762–765. [[CrossRef](#)] [[PubMed](#)]

7. Garcia-Molina, M.M.; Muñoz-Muñoz, J.L.; Garcia-Molina, F.; García-Ruiz, P.A.; Garcia-Canovas, F. Action of Tyrosinase on Ortho-Substituted Phenols: Possible Influence on Browning and Melanogenesis. *J. Agric. Food Chem.* **2012**, *60*, 6447–6453. [[CrossRef](#)] [[PubMed](#)]
8. Ismaya, W.T.; Rozeboom, H.J.; Weijn, A.; Mes, J.J.; Fusetti, F.; Wichers, H.J.; Dijkstra, B.W. Crystal structure of *Agaricus bisporus* mushroom tyrosinase: Identity of the tetramer subunits and interaction with tropolone. *Biochemistry* **2011**, *50*, 5477–5486. [[CrossRef](#)] [[PubMed](#)]
9. Vachtenheim, J.; Borovanský, J. “Transcription physiology” of pigment formation in melanocytes: Central role of MITF. *Exp. Dermatol.* **2010**, *19*, 617–627. [[CrossRef](#)] [[PubMed](#)]
10. Pillaiyar, T.; Manickam, M.; Jung, S.H. Downregulation of melanogenesis: Drug discovery and therapeutic options. *Drug Discov. Today* **2017**, *22*, 282–298. [[CrossRef](#)] [[PubMed](#)]
11. Del Marmol, V.; Beermann, F. Tyrosinase and related proteins in mammalian pigmentation. *FEBS Lett.* **1996**, *381*, 165–168. [[CrossRef](#)]
12. Liu, J.J.; Fisher, D.E. Lighting a path to pigmentation: Mechanisms of MITF induction by UV. *Pigment Cell Melanoma Res.* **2010**, *23*, 741–745. [[CrossRef](#)] [[PubMed](#)]
13. Wu, C.; Sun, Z.; Ye, Y.; Han, X.; Song, X.; Liu, S. Psoralen inhibits bone metastasis of breast cancer in mice. *Fitoterapia* **2013**, *91*, 205–210. [[CrossRef](#)] [[PubMed](#)]
14. Harzallah, A.; Bhourri, A.M.; Amri, Z.; Soltana, H.; Hammami, M. Phytochemical content and antioxidant activity of different fruit parts juices of three figs (*Ficus carica* L.) varieties grown in Tunisia. *Ind. Crops Prod.* **2016**, *83*, 255–267. [[CrossRef](#)]
15. Wang, Y.F.; Liu, Y.N.; Xiong, W.; Yan, D.M.; Zhu, Y.; Gao, X.M.; Xu, Y.T.; Qi, A.D. A UPLC–MS/MS method for in vivo and in vitro pharmacokinetic studies of psoralenoside, isopsoralenoside, psoralen and isopsoralen from *Psoralea corylifolia* extract. *J. Ethnopharmacol.* **2014**, *151*, 609–617. [[CrossRef](#)] [[PubMed](#)]
16. Pei, T.; Zheng, C.; Huang, C.; Chen, X.; Guo, Z.; Fu, Y.; Liu, J.; Wang, Y. Systematic understanding the mechanisms of vitiligo pathogenesis and its treatment by Qubaibabuqi formula. *J. Ethnopharmacol.* **2016**, *190*, 272–287. [[CrossRef](#)] [[PubMed](#)]
17. Jois, H.S.; Manjunath, B.L.; Venkatarao, S. Chemical examination of the seeds of *Psoralea corylifolia*. *J. Indian Chem. Soc.* **1933**, *10*, 41–43.
18. Späth, E. Constitution and synthesis of foeniculin. *Ber. Deut. Chem. Ges.* **1937**, *70*, 83–87. [[CrossRef](#)]
19. Fowucs, W.L.; Griffith, D.G.; Oginsky, E.L. Photosensitization of bacteria by furocoumarins and related compounds. *Nature* **1958**, *181*, 571–572.
20. El Mofty, A.M. *Vitiligo and Psoralens*; Pergamon Press: Oxford, UK, 1968.
21. Fitzpatrick, T.B.; Parrish, J.A.; Pathak, M.A. *Phototherapy of Vitiligo (Idiopathic Leukoderma) in Sunlight and Man*; Tokyo University Press: Tokyo, Japan, 1974.
22. Parrish, J.A.; Fitzpatrick, T.B.; Shea, C.; Pathak, M.A. Photochemotherapy of vitiligo: Use of orally administered psoralens and a high-intensity long-wave ultraviolet light system. *Arch. Dermatol.* **1976**, *112*, 1531–1534. [[CrossRef](#)] [[PubMed](#)]
23. Felsten, L.M.; Alikhan, A.; Petronic-Rosic, V. Vitiligo: A comprehensive overview: Part II: Treatment options and approach to treatment. *J. Am. Acad. Dermatol.* **2011**, *65*, 493–514. [[CrossRef](#)] [[PubMed](#)]
24. Tippisetty, S.; Goudi, D.; Mohammed, A.W.; Jahan, P. Repair efficiency and PUVA therapeutic response variation in patients with vitiligo. *Toxicology* **2013**, *27*, 438–440. [[CrossRef](#)] [[PubMed](#)]
25. Whitton, M.E.; Ashcroft, D.M.; González, U. Therapeutic interventions for vitiligo. *J. Am. Acad. Dermatol.* **2008**, *59*, 713–717. [[CrossRef](#)] [[PubMed](#)]
26. Niu, C.; Aisa, H.A. Upregulation of Melanogenesis and Tyrosinase Activity: Potential Agents for Vitiligo. *Molecules* **2017**, *22*. [[CrossRef](#)] [[PubMed](#)]
27. Niu, C.; Li, G.; Tuerxuntayi, A.; Aisa, H.A. Synthesis and Bioactivity of New Chalcone Derivatives as Potential Tyrosinase Activator Based on the Click Chemistry. *Chin. J. Chem.* **2015**, *33*, 486–494. [[CrossRef](#)]
28. Niu, C.; Pang, G.X.; Li, G.; Dou, J.; Nie, L.F.; Himit, H.; Kabas, M.; Aisa, H.A. Synthesis and biological evaluation of furocoumarin derivatives on melanin synthesis in murine B16 cells for the treatment of vitiligo. *Biorg. Med. Chem.* **2016**, *24*, 5960–5968. [[CrossRef](#)] [[PubMed](#)]
29. Niu, C.; Tuerxuntayi, A.; Li, G.; Kabas, M.; Dong, C.Z.; Aisa, H.A. Design, synthesis and bioactivity of chalcones and its analogues. *Chin. Chem. Lett.* **2017**, *28*, 1533–1538. [[CrossRef](#)]

30. Niu, C.; Yin, L.; Nie, L.F.; Dou, J.; Zhao, J.Y.; Li, G.; Aisa, H.A. Synthesis and bioactivity of novel isoxazole chalcone derivatives on tyrosinase and melanin synthesis in murine B16 cells for the treatment of vitiligo. *Biorg. Med. Chem.* **2016**, *24*, 5440–5448. [[CrossRef](#)] [[PubMed](#)]
31. Niu, C.; Li, G.; Madina, K.; Aisa, H.A. Synthesis and activity on tyrosinase of novel chalcone derivatives. *Chem. J. Chin. Univ.* **2014**, *35*, 1204–1211. [[CrossRef](#)]
32. Zhang, B.L.; Fan, C.Q.; Dong, L.; Wang, F.D.; Yue, J.M. Structural modification of a specific antimicrobial lead against *Helicobacter pylori* discovered from traditional Chinese medicine and a structure–activity relationship study. *Eur. J. Med. Chem.* **2010**, *45*, 5258–5264. [[CrossRef](#)] [[PubMed](#)]
33. Zhang, Y.; Zou, B.; Chen, Z.; Pan, Y.; Wang, H.; Liang, H.; Yi, X. Synthesis and antioxidant activities of novel 4-Schiff base-7-benzyloxy-coumarin derivatives. *Bioorg. Med. Chem. Lett.* **2011**, *21*, 6811–6815. [[CrossRef](#)] [[PubMed](#)]
34. Shen, Q.; Peng, Q.; Shao, J.L.; Liu, X.F.; Huang, Z.S.; Pu, X.Z.; Ma, L.; Li, Y.M.; Chan, A.S.C.; Gu, L.Q. Synthesis and biological evaluation of functionalized coumarins as acetylcholinesterase inhibitors. *Eur. J. Med. Chem.* **2005**, *40*, 1307–1315. [[CrossRef](#)] [[PubMed](#)]
35. Schönleber, R.O.; Bendig, J.; Hagen, V.; Giese, B. Rapid photolytic release of cytidine 5'-diphosphate from a coumarin derivative: A new tool for the investigation of ribonucleotide reductases. *Biorg. Med. Chem.* **2002**, *10*, 97–101. [[CrossRef](#)]
36. Fournier, L.; Aujard, I.; Le Saux, T.; Maurin, S.; Beaupierre, S.; Baudin, J.B.; Jullien, L. Coumarinylmethyl Caging Groups with Redshifted Absorption. *Chem. Eur. J.* **2013**, *19*, 17494–17507. [[CrossRef](#)] [[PubMed](#)]
37. Kim, H.J.; Kim, J.S.; Woo, J.T.; Lee, I.S.; Cha, B.Y. Hyperpigmentation mechanism of methyl 3,5-di-caffeoylquinic acid through activation of p38 and MITF induction of tyrosinase. *Acta Biochim. Biophys. Sin.* **2015**, *47*, 548–556. [[CrossRef](#)] [[PubMed](#)]
38. Bellei, B.; Flori, E.; Izzo, E.; Maresca, V.; Picardo, M. GSK3 β inhibition promotes melanogenesis in mouse B16 melanoma cells and normal human melanocytes. *Cell. Signal.* **2008**, *20*, 1750–1761. [[CrossRef](#)] [[PubMed](#)]
39. Bellei, B.; Pitisci, A.; Catricalà, C.; Larue, L.; Picardo, M. Wnt/ β -catenin signaling is stimulated by α -melanocyte-stimulating hormone in melanoma and melanocyte cells: Implication in cell differentiation. *Pigment Cell Melanoma Res.* **2011**, *24*, 309–325. [[CrossRef](#)] [[PubMed](#)]
40. Takeda, K.; Takemoto, C.; Kobayashi, I.; Watanabe, A.; Nobukuni, Y.; Fisher, D.E.; Tachibana, M. Ser298 of MITF, a mutation site in Waardenburg syndrome type 2, is a phosphorylation site with functional significance. *Hum. Mol. Genet.* **2000**, *9*, 125–132. [[CrossRef](#)] [[PubMed](#)]
41. Debowska, R.; Pasikowska, M.; Bazela, K.; Szczepanowska, J.; Ciescinska, C.; Vincent, C.; Napierala, M.; Szewczyk, A.; Lewandowska, M.; Eris, I. Plant flavonoid activating potassium channels—Naringenin for vitiligo skin care. *J. Investig. Dermatol.* **2016**, *136*. [[CrossRef](#)]
42. Lin, J.J.; Yu, J.; Zhao, J.Y.; Zhang, K.; Zheng, J.C.; Wang, J.L.; Huang, C.H.; Zhang, J.R.; Yan, X.J.; Gerwick, W.H.; et al. Fucoxanthin, a Marine Carotenoid, Attenuates beta-Amyloid Oligomer-Induced Neurotoxicity Possibly via Regulating the PI3K/Akt and the ERK Pathways in SH-SY5Y Cells. *Oxid. Med. Cell. Longev.* **2017**, *2017*, 6792543. [[CrossRef](#)] [[PubMed](#)]
43. Ma, J.W.; Wang, Z.; Liu, C.L.; Shen, H.T.; Chen, Z.Q.; Yin, J.; Zuo, G.; Duan, X.C.; Li, H.Y.; Chen, G. Pramipexole-Induced Hypothermia Reduces Early Brain Injury via PI3K/AKT/GSK3 β pathway in Subarachnoid Hemorrhage rats. *Sci. Rep.* **2016**, *6*, 23817. [[CrossRef](#)] [[PubMed](#)]
44. Sun, Y.J.; Song, D.D.; Wang, M.; Chen, K.Y.; Zhang, T.Z. Alpha7 nicotinic acetylcholine receptor agonist attenuates the cerebral injury in a rat model of cardiopulmonary bypass by activating the Akt/GSK3beta pathway. *Mol. Med. Rep.* **2017**, *16*, 7979–7986. [[CrossRef](#)] [[PubMed](#)]
45. Wang, X.; Zhao, L.H. Calycosin ameliorates diabetes-induced cognitive impairments in rats by reducing oxidative stress via the PI3K/Akt/GSK-3 β signaling pathway. *Biochem. Biophys. Res. Commun.* **2016**, *473*, 428–434. [[CrossRef](#)] [[PubMed](#)]
46. Zong, Z.K.; Pang, H.; Yu, R.T.; Jiao, Y.Q. PCDH8 inhibits glioma cell proliferation by negatively regulating the AKT/GSK3beta/beta-catenin signaling pathway. *Oncol. Lett.* **2017**, *14*, 3357–3362. [[CrossRef](#)] [[PubMed](#)]
47. Kim, H.J.; Park, S.Y.; Park, O.J.; Kim, Y.M. Curcumin suppresses migration and proliferation of Hep3B hepatocarcinoma cells through inhibition of the Wnt signaling pathway. *Mol. Med. Rep.* **2013**, *8*, 282–286. [[CrossRef](#)] [[PubMed](#)]
48. Yam, J.W.; Wong, C.M.; Ng, I.O. Molecular and functional genetics of hepatocellular carcinoma. *Front. Biosci.* **2010**, *2*, 117–134.

49. Fukuda, K.; Hibiya, Y.; Mutoh, M.; Koshiji, M.; Akao, S.; Fujiwara, H. Inhibition by berberine of cyclooxygenase-2 transcriptional activity in human colon cancer cells. *J. Ethnopharmacol.* **1999**, *66*, 227–233. [[CrossRef](#)]
50. Kong, W.J.; Wei, J.; Abidi, P.; Lin, M.H.; Inaba, S.; Li, C.; Wang, Y.L.; Wang, Z.Z.; Si, S.Y.; Pan, H.N.; et al. Berberine is a novel cholesterol-lowering drug working through a unique mechanism distinct from statins. *Nat. Med.* **2004**, *10*, 1344. [[CrossRef](#)] [[PubMed](#)]
51. Yang, J.; Yin, J.H.; Gao, H.F.; Xu, L.X.; Wang, Y.; Xu, L.; Li, M. Berberine improves insulin sensitivity by inhibiting fat store and adjusting adipokines profile in human preadipocytes and metabolic syndrome patients. *Evid.-Based Complement. Alternat. Med.* **2012**, *2012*, 363845. [[CrossRef](#)] [[PubMed](#)]
52. Lee, J.; Jung, K.; Kim, Y.S.; Park, D. Diosgenin inhibits melanogenesis through the activation of phosphatidylinositol-3-kinase pathway (PI3K) signaling. *Life Sci.* **2007**, *81*, 249–254. [[CrossRef](#)] [[PubMed](#)]
53. Ko, H.H.; Tsai, Y.T.; Yen, M.H.; Lin, C.C.; Liang, C.J.; Yang, T.H.; Lee, C.W.; Yen, F.L. Norartocarpetin from a folk medicine *Artocarpus communis* plays a melanogenesis inhibitor without cytotoxicity in B16F10 cell and skin irritation in mice. *BMC Complement. Alternat. Med.* **2013**, *13*, 348. [[CrossRef](#)] [[PubMed](#)]
54. Lee, D.H.; Kim, D.H.; Oh, I.Y.; Kim, S.Y.; Lim, Y.Y.; Kim, H.M.; Kim, Y.H.; Choi, Y.M.; Kim, S.E.; Kim, B.J.; et al. Inhibitory Effects of *Saururi chinensis* Extracts on Melanin Biosynthesis in B16F10 Melanoma Cells. *Biol. Pharm. Bull.* **2013**, *36*, 772–779. [[CrossRef](#)] [[PubMed](#)]



© 2018 by the authors. Licensee MDPI, Basel, Switzerland. This article is an open access article distributed under the terms and conditions of the Creative Commons Attribution (CC BY) license (<http://creativecommons.org/licenses/by/4.0/>).